Influence of Lignosulfonate on the Hydrothermal Interaction Between Pyrite and Cu(II) Ions in Sulfuric Acid Media

Kirill Karimov , Maksim Tretiak * , Uliana Sharipova , Tatiana Lugovitskaya , Oleg Dizer , Denis Rogozhnikov

Posted Date: 19 December 2025

doi: 10.20944/preprints202512.1809.v1

Keywords: pyrite; hydrothermal treatment; copper sulfides; sodium lignosulfonate; surfactant; autoclave leaching; mine tailings

 doi:10.20944/preprints202512.1809.v1

Article

Influence of Lignosulfonate on the Hydrothermal Interaction Between Pyrite and Cu(II) Ions in Sulfuric Acid Media

Kirill Karimov, Maksim Tretiak *, Uliana Sharipova, Tatiana Lugovitskaya, Oleg Dizer and Denis Rogozhnikov

Laboratory of Advanced Technologies in Non-Ferrous and Ferrous Metals Raw Materials Processing, Institute of New Materials and Technologies, Ural Federal University Named After the First President of Russia B.N. Yeltsin (UrFU), 620002 Yekaterinburg, Russia

* Correspondence: m.a.tretiak@urfu.ru

Abstract

Hydrometallurgical pretreatment of pyrite-bearing concentrates and tailings by hydrothermal interaction with Cu(II) solutions is a promising route for chemical beneficiation and mitigation of acid mine drainage but is limited by passivation caused by elemental sulfur and secondary copper sulfides. Here, the effect of sodium lignosulfonate (SLS) on the hydrothermal reaction between natural pyrite and $CuSO_4$ in H_2SO_4 media at 180–220 °C was studied at $[H_2SO_4]_0$ = 10–30 g/dm^3, $[Cu]_0$ = 6–24 g/dm^3 and $[SLS]_0$ = 0–1.0 g/dm^3. Process efficiency was evaluated by Fe extraction into solution and Cu precipitation on the solid phase, and products were characterized by XRD and SEM/EDS. SLS markedly intensified pyrite conversion: at 200 °C and 120 min Fe extraction increased from 14 to 26 % and Cu precipitation from 5 to 23 %, while at 220 °C Fe extraction reached 33.4 % and Cu precipitation 26.8 %. XRD confirmed the sequential transformation CuS → $Cu_{1.8}S$. SEM/EDS showed that SLS converts localized nucleation of Cu_xS on defect sites into the formation of a fine, loosely packed and well-dispersed copper sulfide phase. The results demonstrate that lignosulfonate surfactants efficiently suppress passivation and enhance mass transfer, providing a basis for intensifying hydrothermal pretreatment of pyrite-bearing industrial materials.

Keywords: pyrite; hydrothermal treatment; copper sulfides; sodium lignosulfonate; surfactant; autoclave leaching; mine tailings

1. Introduction

The global mining industry continues to expand production to meet growing demand for metals. In particular, annual copper ore production has increased by an average of 2.2–2.5 %, reaching ~20 million tons in recent years [1]. Pyrometallurgy remains the primary method for processing copper concentrates because it ensures high productivity and efficient extraction of associated precious metals [2,3]. The greatest economic benefits are achieved by companies that cover the entire production cycle, from copper mining to refining [4,5]. However, tightening environmental regulations and growing interest in waste-free technologies are stimulating the modernization of existing production facilities, including the introduction of modern exhaust gas cleaning systems and the integrated processing of slags and dusts [6–9]. In this context, hydrometallurgical alternatives, regarded as more environmentally friendly solutions, attract increasing attention, setting the stage for rethinking approaches to managing beneficiation tailings and processing problematic mineral phases [10].

Froth flotation is the primary method for beneficiating sulfide ores, particularly chalcopyrite ores [6]. However, its selectivity decreases when processing ores with fine dissemination and complex mineralogical intergrowths of valuable and gangue minerals [11]. The presence of pyrite in

 doi:10.20944/preprints202512.1809.v1

concentrates and tailings is one of the key technological problems. This occurs due to its activation by copper ions, which could be released from secondary copper minerals or added to the process as an activating reagent for sphalerite [12–15]. As a result, pyrite, along with its impurities (Zn, Pb, As, etc.), passes either into the final concentrate, reducing its quality and market value, or into the tailings, increasing their environmental hazard [10]. Interestingly, in complex systems containing sphalerite, the latter can act as a copper sink, leading to pyrite depression [16,17]. Consequently, there is a need to develop novel methods which would selectively modify or remove the sulfide phase, primarily pyrite, just after primary enrichment.

Mine tailings are finely ground rock material remaining after the extraction of valuable components from ore [18]. Globally, they are produced in excess of 20 billion tons per year, and the total area of tailings storage facilities is estimated at over 200,000 km² [19,20]. The primary environmental hazard associated with mine tailings is the presence of residual sulfide minerals, primarily pyrite (FeS_2). When exposed to atmospheric oxygen and precipitation, pyrite oxidizes, producing sulfuric acid and acid mine drainage. This process significantly increases the mobility of heavy metals, causing contamination of soils, surface water, and groundwater. Furthermore, the instability of tailings storage structures creates the risk of catastrophic failures, as demonstrated by accidents at Mount Polley (Canada), Brumadinho and Mariana (Brazil), which resulted in widespread and long-term environmental damage [21,22]. Since the source of both acidity and toxicity is the sulfide fraction, primarily pyrite, managing its behavior in tailings is key to reducing environmental risks.

The use of hydrometallurgical technologies as a method for chemical enrichment or purification of concentrates and tailings is a promising approach to addressing these issues [23–29]. The method involves the interaction of undesirable pyrite (FeS_2) with copper ions in aqueous solutions at elevated temperatures to form secondary copper sulfides (CuS, $Cu_{1.8}S$, Cu_2S) [30,31]. However, the high chemical stability of pyrite is the main challenge in implementing this approach. Numerous studies show that its significant conversion is achieved at high temperatures only, typically above 225–240 °C, while it remains virtually inert at temperatures below 200 °C [32–34].

Controlling this process requires a deep understanding of the fundamental mechanisms of pyrite interaction with copper ions in various aqueous media, which is supported by a number of key studies. For example, Kritsky et al. [35] present a detailed kinetic analysis of the process in an acidic sulfate medium using pyrite with particle sizes of 10–29 μm. The process was studied in the temperature range of 443–523 K (170–250°C) at $CuSO_4$ concentrations of 0.08–0.96 mol/L and H_2SO_4 concentrations of 0.05–0.6 mol/L. It has been established that an exchange reaction proceeds at the initial stage:

$$FeS_2 + 1.75Cu^{2+} + H_2O \longrightarrow 1.75CuS + Fe^{2+} + 2H^+ + 0.25SO_4^{2-} \quad (1)$$

Significant pyrite conversion (up to 50 %) is achieved at temperatures above 250 °C only. The process kinetics were found to be two-stage, with activation energies of 61.1 kJ/mol and 37.0 kJ/mol, respectively, indicating internal diffusion control limited by the formation of a dense product film (Kp-B > 1) from successive layers of CuS, $Cu_{1.8}S$, and Cu_2S.

In contrast, a study by Zhang et al. [36] in a chloride medium showed a different mechanism when working with natural pyrite crystals (~2 mm, Shanbao deposit) within 100–250°C and pH from 1 to 8. Here, coupled dissolution-precipitation dominates, including reductive precipitation and oxidative dissolution;

$$14FeS_2 + 14CuCl_2^- + 14e^- \longrightarrow 14CuFeS_2 + 28Cl^- \quad (2)$$

$$FeS_2 + 8H_2O + 2Cl^- \longrightarrow 14H^+ + FeCl_2(aq) + 2HSO_4^- + 14e^- \quad (3)$$

The composition of the products is tightly controlled by pH, namely: within pH 3.0–6.0, chalcopyrite and bornite are formed, while chalcocite and bornite are formed at pH 8.2, forming a zonal structure from the pyrite core to the surface. Diffusion through the product layers is the limiting factor here.

 doi:10.20944/preprints202512.1809.v1

Supplementing these data, Fuentes et al. [30] also investigated the sulfate system using pyrite with a purity of 95–98 % (25–40 μm, Navahun deposit) at 180–240°C and pH 1.1–1.4. It was found that conversion of up to 47 % in 2 h is achieved at 240°C only, and the process is controlled by a chemical reaction (activation energy ~110 kJ/mol). The reaction products are digenite ($Cu_{1.8}S$) and chalcocite, and the resulting layer is porous (Kp-B ≈ 1.6), facilitating the access of reagents.

Thus, our analysis of the literature shows that the hydrothermal conversion of pyrite is a complex multifactorial process, and despite a significant volume of research, few questions regarding its adaptation to heterogeneous technogenic materials remain open [37,38]. The kinetics of the process are controlled by a complex combination of diffusion and chemical factors, and a dense layer of reaction products forms on the mineral surface, slowing further interaction with reagents. The complexity of the mechanism, which depends on pH, temperature, and solution composition, as well as the high stability of pyrite, necessitate further fundamental study of its behavior under hydrothermal conditions to develop effective technologies for processing pyrite-containing industrial products.

The passivation layer, which shields the mineral surface from reagents, creates a kinetic barrier and may lead to the complete cessation of the leaching reaction by limiting pyrite interaction with the reagents [39]. This phenomenon creates a technological demand for the use of surface-active additives (surfactants) capable of removing sulfur films and other solid reaction products and stabilizing dispersion in the system[40].

Lignosulfonates (LS) have proven themselves to be highly effective and cost-effective reagents for solving the problem of passivation of the surface of sulfide minerals. They act as sulfur dispersants and modifiers of the interfacial properties of the system. Their mechanism of action involves adsorption at the interfaces, which leads to a decrease in interfacial tension at the liquid sulfur–aqueous solution boundary and a reduction in the work of adhesion of sulfur to the mineral surface [41,42]. By adsorbing at the mineral–solution and sulfur–solution boundaries, they make the mineral surface more hydrophilic and less easily wetted by sulfur [43]. This prevents sulfide particles from being coated with molten sulfur and intensifies the leaching process. Due to their effectiveness, availability, and non-toxicity, lignosulfonates have found widespread industrial application, including pressure leaching of sulfide concentrates [44,45].

Under hydrothermal conditions characterized by elevated temperatures and pressures, managing interfacial phenomena such as wetting and adsorption becomes critical to suppressing sulfide surface passivation and maintaining high rates of mass and charge transfer. The use of lignosulfonates under these conditions is an effective tool for reducing sulfide surface passivation, ensuring reagent access and intensifying the recovery process. For example, in oxidative pressure leaching of sulfides in a sulfuric acid medium, the addition of lignosulfonates prevents the encapsulation of sulfide particles by molten elemental sulfur. This removes the kinetic barrier and achieves a higher recovery rate, exceeding 95 % [46,47].

Under hydrothermal conditions, lignosulfonate acts as a dispersant, effectively removing molten sulfur from the mineral surface and altering the solid residue morphology [48]. Instead of the characteristic spherical sulfur agglomerates formed in the absence of surfactants, particles with a rougher surface form in its presence [49]. The key mechanisms of lignosulfonate action in pressure leaching processes involve a sequence of colloidal chemical processes, including wetting, adsorption, and dispersion. Adsorption of lignosulfonates at the elemental sulfur–solution and mineral–solution interfaces leads to a decrease in their surface tension. The combination of these effects transforms the system from a regime of mineral wetting by molten sulfur to that of poorly wetted sulfur surface protected by an adsorbed lignosulfonate layer and stabilized dispersion of sulfur in the solution.

Therefore, this study aimed to investigate the influence of lignosulfonate on the interaction of pyrite with copper ions under hydrothermal conditions, the composition of the resulting products, and surface phenomena.

 doi:10.20944/preprints202512.1809.v1

2. Materials and Methods

2.1. Analysis

Chemical analysis of the starting minerals and the resulting solid dissolution products was performed using an ARL Advant'X 4200 wavelength-dispersive spectrometer (Thermo Fisher Scientific Inc., Waltham, MA, USA). Phase analysis was carried out on an XRD 7000 Maxima diffractometer (Shimadzu Corp., Tokyo, Japan).

Particle size analysis was performed using laser diffraction on an Analysette 22 Nanotec Plus (FRITSCH GmbH, Idar-Oberstein, Germany).

Chemical analysis of the resulting solutions was done using inductively coupled plasma mass spectrometry (ICP-MS) on an Elan 9000 instrument (PerkinElmer Inc., Waltham, MA, USA).

Scanning electron microscopy (SEM) was performed using a JSM-6390LV microscope (JEOL Ltd., Tokyo, Japan) equipped with a module for energy-dispersive X-ray spectroscopy analysis (EDX).

2.2. Materials and Reagents

The main raw material used was the natural sulfide mineral pyrite, obtained from the Berezovskoye deposit (Sverdlovsk region, RF). Figure 1 shows X-ray diffraction patterns of the minerals. All minerals were crushed and sieved on laboratory sieves. After sieving, the material was ground to P80 = 40 μm (80 % passing 40 μm).

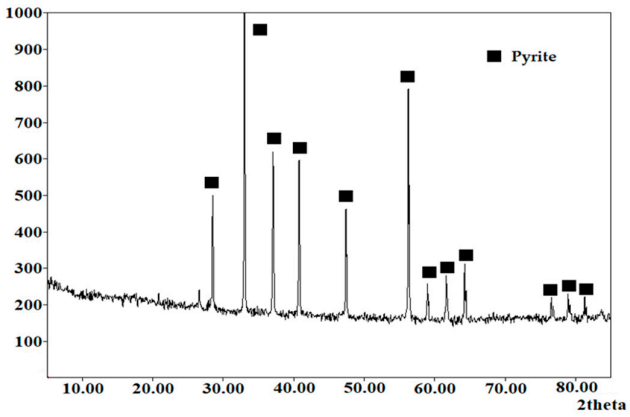

Figure 1. X-ray diffraction pattern of the pyrite used.

The particle size distribution of the minerals is shown in Figure 2.

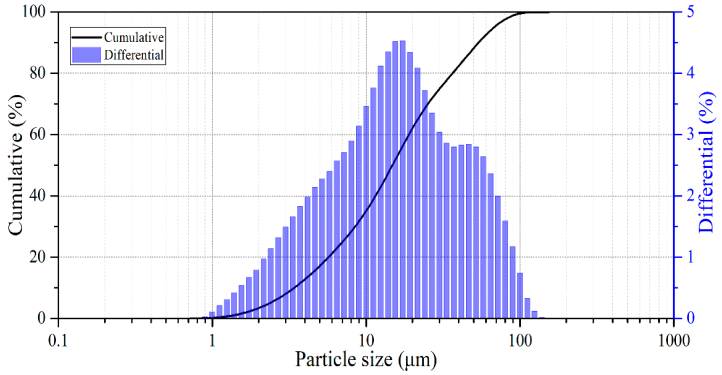

Figure 2. Particle size distribution of crushed pyrite.

 doi:10.20944/preprints202512.1809.v1

The percentage content of the d_{10}, d_{50} and d_{90} fractions was 3.41, 14.81, and 53.77 μm, respectively. The chemical composition of pyrite was 44.1 wt.% Fe, 50.8 wt.% S, and 5.1 wt.% others. All other reagents were of analytical grade.

2.2. Experimental Equipment and Procedures

Laboratory pressure leaching experiments were conducted in a 1.0 dm^3 titanium autoclave (Parr Instrument, Moline, IL, USA) with temperature control within ±2 °C. Stirring was provided by an overhead stirrer to ensure pulp homogeneity.

Before the experiment, a 600 cm^3 solution containing H_2SO_4 and $CuSO_4$ at specified concentrations was prepared. The autoclave filling factor was 0.6. After loading the pulp, the reactor was sealed, the stirrer was started, and the pulp was heated to the required temperature. The stirrer speed was maintained at 800 rpm, ensuring a uniform pulp density. Upon reaching the specified temperature, the pyrite pulp was added, and the experiment was initiated. At the end of the experiment and the autoclave was cooled down to 70 °C. The pulp was filtered; the cake was washed and dried to constant weight. Samples were taken from the liquid and solid products for analysis.

3. Results and Discussion

To optimize the autoclave processing, it is necessary to understand the interaction of pyrite with copper sulfate in sulfuric acid solutions. The behavior of FeS_2 is known from the literature; however, information on the behavior of this mineral in the presence of surfactants is lacking.

The reactions describing the autoclave processing of the pyrite are presented below:

$$FeS_2 + CuSO_4 \rightarrow CuS + FeSO_4 + S^0 \quad (4)$$

$$4FeS_2 + 7CuSO_4 + 4H_2O \rightarrow 7CuS + 4FeSO_4 + 4H_2SO_4 \quad (5)$$

$$5FeS_2 + 14CuSO_4 + 12H_2O \rightarrow 7Cu_2S + 5FeSO_4 + 12H_2SO_4 \quad (6)$$

$$FeS_2 + 2.61CuSO_4 + 2.16H_2O \rightarrow 1.45Cu_{1.8}S + FeSO_4 + 2.16\ H_2SO_4 \quad (7)$$

$$5CuS + 3CuSO_4 + 4\ H_2O \rightarrow 4Cu_2S + 4H_2SO_4 \quad (8)$$

$$6CuSO_4 + 5S^0 + 8H_2O \rightarrow 7Cu_2S + 8H_2SO_4 \quad (9)$$

This section is devoted to studying the effectiveness of sodium lignosulfonate (SLS) as a surfactant in the autoclave processing of pyrite. The study aims to establish quantitative relationships between the main process parameters and copper precipitation and pyrite recovery indicators. In particular, the kinetics of pyrite dissolution with the release of iron ions into solution is examined in detail.

The experiments were conducted under high hydrothermal conditions (180–220 °C). It should be emphasized that the presented results are unique: the influence of SLS on phase transformations during the interaction of copper sulfate solutions with pyrite in the specified temperature range has not previously been described in the literature.

The influence of key process parameters on the degree of interaction of pyrite with copper (II) ions under hydrothermal conditions was studied. Variable factors included process temperature (180–220 °C), the initial concentration of sulfuric acid (10–30 g/dm^3), copper (II) (6–24 g/dm^3) and SLS (0.25–1.00 g/dm^3).

The efficiency of pyrite conversion was assessed based on the degree of iron transfer into solution and the amount of copper precipitation on the solid phase surface. This approach allows for a comprehensive characterization of both FeS_2 dissolution and the accompanying redox exchange processes between pyrite and Cu (II), which is particularly important when analyzing the behavior of minerals in complex sulfate systems.

 doi:10.20944/preprints202512.1809.v1

3.1. Effect of Sodium Lignosulfonate

Figure 3 shows the effect of SLS concentration on the degree of iron extraction and the degree of copper precipitation during hydrothermal treatment of pyrite.

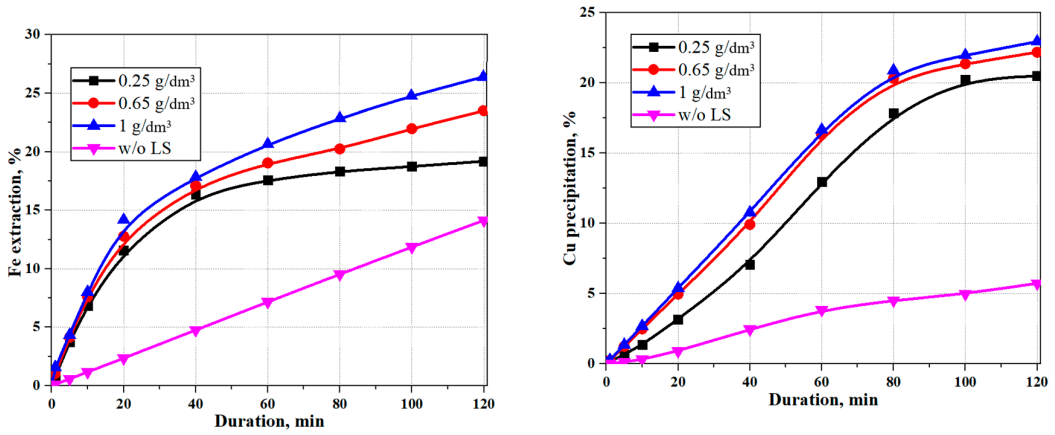

(**a**) (**b**)

Figure 3. Effect of initial lignosulfonate concentration during hydrothermal pyrite treatment: (**a**) extraction iron; (**b**) copper precipitation. (t = 200°C, $[H_2SO_4]_0$ = 20 g/dm³, $[Cu]_0$ = 15 g/dm³).

The graph shows a significant effect of sodium lignosulfonate addition on iron extraction from pyrite and copper precipitation onto pyrite. As with sphalerite, the addition of sodium lignosulfonate significantly intensifies the hydrothermal treatment of pyrite. Increasing the initial lignosulfonate concentration moderately increases iron extraction. After 120 min of hydrothermal treatment with 0.25 g/dm³ and 1 g/dm³ lignosulfonate, iron extraction was 19 % and 26 %, respectively, compared to 14 % without sodium lignosulfonate. Copper precipitation also increases with increasing initial sodium lignosulfonate concentration, namely: after 120 min without sodium lignosulfonate, with 0.25 g/dm³ and 1 g/dm³, copper precipitation was 5 %, 20 %, and 23 %, respectively. For the following calculations, an initial SLS concentration of 1 g/dm³ was adopted.

Analysis of the experimental data (Figure 3) showed that sodium lignosulfonate (SLS) has a significant impact on iron extraction and the concomitant copper deposition on the pyrite surface. SLS introduction significantly intensifies the hydrothermal interaction of pyrite with copper (II) ions.

With increasing initial SLS concentration, an increase in the degree of iron release into solution is observed. After 120 min of hydrothermal treatment at SLS concentrations of 0.25 and 1.0 g/dm³, iron extraction was 19 % and 26 %, respectively, while it did not exceed 14 % in the control experiment without surfactants. A similar trend is observed for the copper precipitation process, namely: the degree of Cu (II) precipitation increases from 5 % (without SLS) up to 20 % at an SLS concentration of 0.25 g/dm³ and up to 23 % at 1.0 g/dm³ over 120 min.

Given the significant increase in the system's reactivity and the most pronounced effect at 1.0 g/dm³, an initial SLS concentration of 1 g/dm³ was adopted for further experiments and modeling.

3.2. Effect of Temperature

Figure 4 shows the effect of temperature on the degree of iron extraction and copper precipitation.

 doi:10.20944/preprints202512.1809.v1

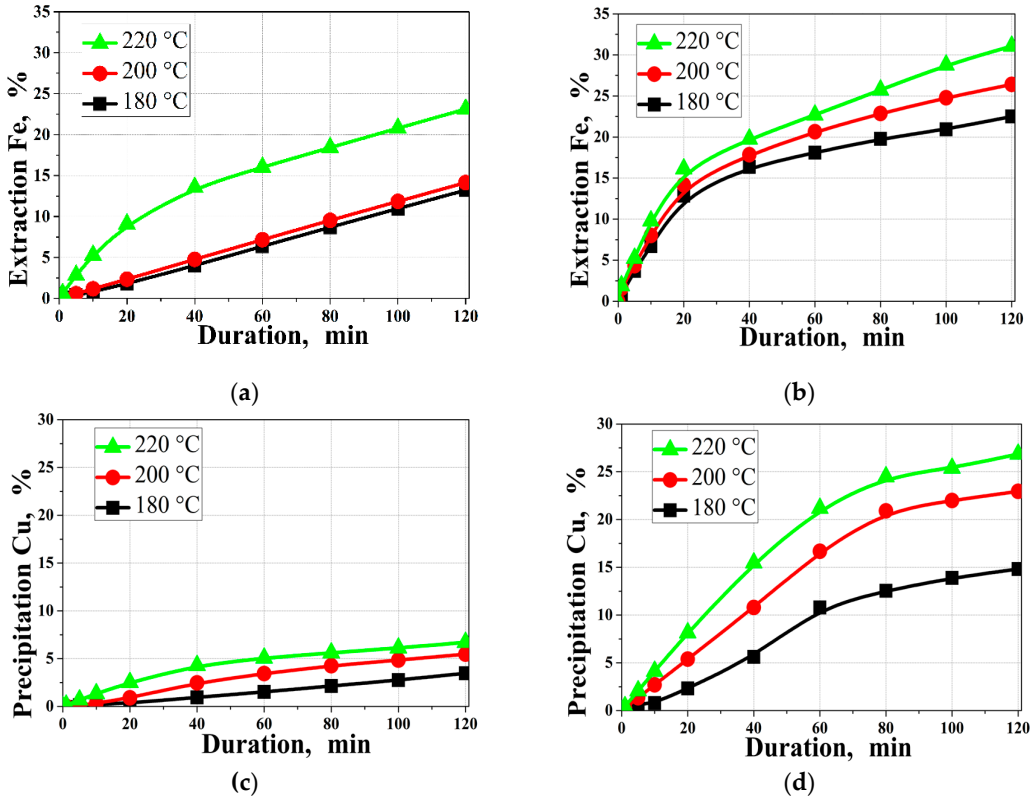

Figure 4. Effect of temperature on the degree on: (**a,b**) iron extraction; (**c,d**) copper precipitation; (**a,c**) in the absence; (**b,d**) in the presence of SLS. ($[H_2SO_4]_0$ = 20 g/dm^3, $[Cu]_0$ = 15 g/dm^3, $[SLS]_0$ = 1 g/dm^3).

As can be seen from the data presented in Figure 4, increasing temperature has a pronounced positive effect on iron extraction into solution and the degree of copper precipitation on the solid phase surface. In the presence of sodium lignosulfonate (SLS) at 220 °C, 33.4 % of the iron is released into solution within 120 min, compared to only 23.1 % in the absence of SLS. Thus, the addition of SLS intensifies the sulfide matrix destruction and iron release into solution.

A similar pattern is observed for copper. The presence of SLS significantly increases its precipitation rate. At temperatures of 180, 200, and 220 °C with no addition of SLS, the copper precipitation rate is 3.5, 5.5, and 6.7 %, respectively after 120 min of treatment. The addition of SLS leads to a sharp increase in this rate—up to 14.8, 22.9, and 26.8 %, respectively, at the same temperatures. This behavior indicates the nature of the influence of SLS, likely related to modification of the surface properties of mineral particles and accelerated reagent transfer.

Based on the obtained dependencies, a temperature of 220 °C was adopted for subsequent experiments as providing the greatest process intensity.

3.3. Effect of Initial Sulfuric Acid Concentration in Solution

Figure 5 shows the effect of the initial sulfuric acid concentration on the degree of iron extraction and copper precipitation.

 doi:10.20944/preprints202512.1809.v1

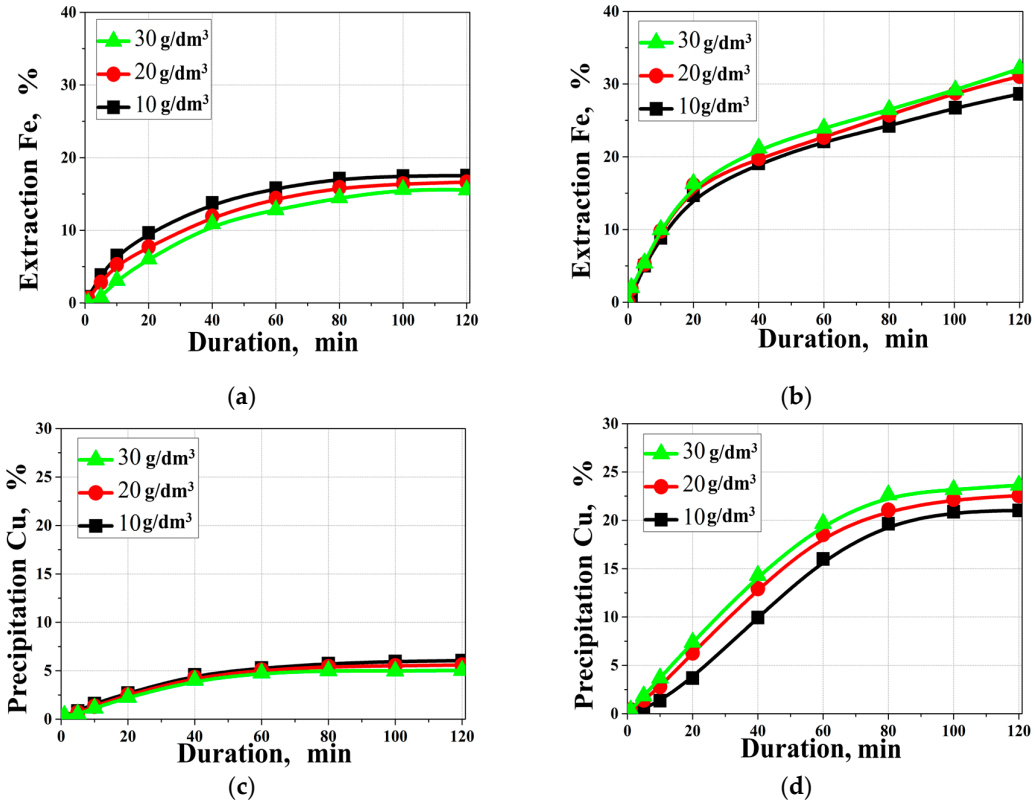

Figure 5. Effect of the initial sulfuric acid concentration on: (**a,b**) iron extraction; (**c,d**) copper precipitation; (**a,c**) in the absence; (**b,d**) in the presence of SLS. (t = 220 °C, $[Cu]_0$ = 15 g/dm³; $[SLS]_0$ = 1 g/dm³).

According to the data presented in Figure 5, the change in the degree of iron extraction from pyrite and copper precipitation indicates that SLS exhibits pronounced dispersing and adsorption properties, which help reduce the passivating effect of elemental sulfur, covellite, digenite on the surface of mineral particles and, consequently, increase the availability of active sites for reactions.

In the absence of SLS, increasing the initial sulfuric acid concentration leads to a decrease in iron extraction and copper precipitation, which is consistent with the concept of enhanced surface passivation at elevated acidity. Conversely, in the presence of SLS, increasing the acid concentration from 10 up to 30 g/dm³ is accompanied by a small but steady increase in the degree of conversion. E.g., after 120 min of hydrothermal treatment of pyrite at 10, 20, and 30 g/dm³ sulfuric acid, 31.3, 33.4, and 33.9 % Fe are extracted, respectively, while copper precipitation reaches 21, 22.5, and 23.6 %, respectively.

These data demonstrate that the use of SLS not only compensates for the negative effect of increased acidity but also ensures more stable oxidation and precipitation reactions. Based on the maximum achieved iron recovery and copper precipitation values, an initial sulfuric acid concentration of 30 g/dm³ was adopted for subsequent experiments.

3.4. Effect of Initial Copper Concentration

Figure 6 shows the effect of the initial copper concentration on iron recovery and copper precipitation.

 doi:10.20944/preprints202512.1809.v1

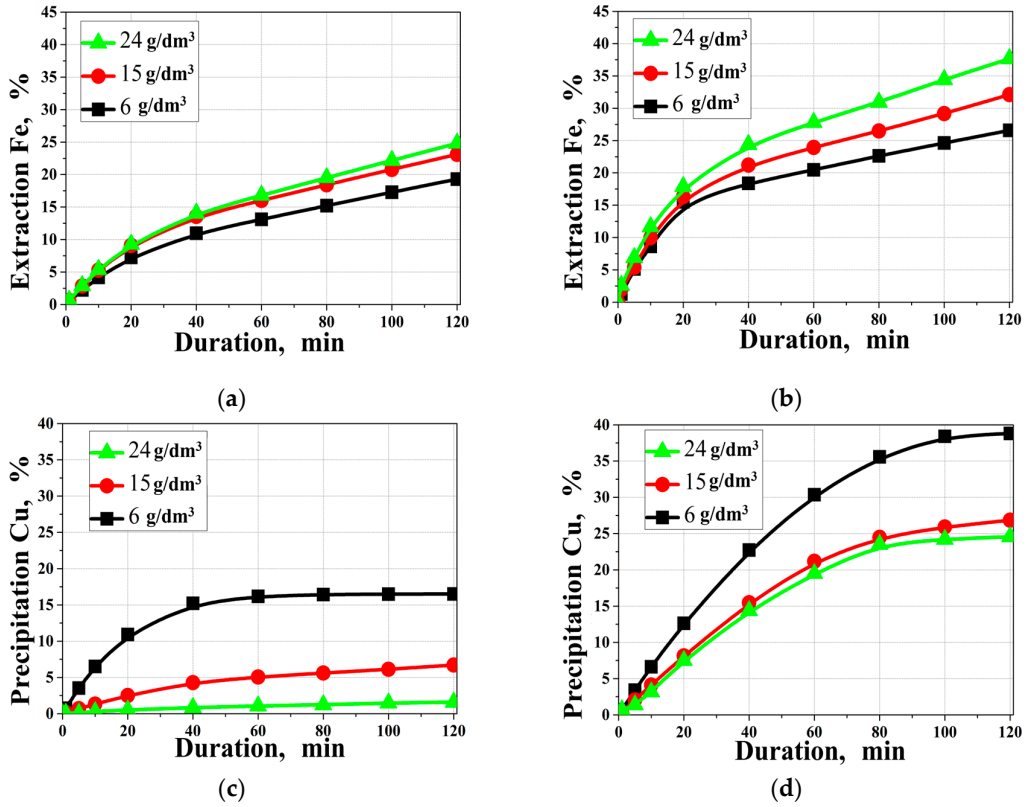

Figure 6. Effect of the initial copper concentration on: (**a,b**) iron Extraction; (**c,d**) copper precipitation; (**a,c**) in the absence; (**b,d**) in the presence of SLS. ($[H_2SO_4]_0$ = 30 g/dm³; t = 220°C; $[SLS]_0$ = 1 g/dm³).

According to Figure 6, increasing the initial copper (II) ion concentration leads to an increase in iron recovery in both the absence and presence of SLS. However, the magnitude of the effect is significantly greater in systems with SLS. E.g., at a copper (II) ion concentration of 24 g/dm³, 41.2 % of Fe is recovered after 120 min of hydrothermal treatment, compared to only 25 % in the system without surfactants. This indicates an increased role for copper as an oxidizer and that SLS facilitates reagent access to the pyrite surface, reducing the effect of passivating films.

Interestingly, copper behavior in solution exhibits a different trend, namely: at an initial concentration of 6 g/dm³, its precipitation rate is 38.8 %, while at 24 g/dm³, it decreases down to 24 %. Despite this, both values significantly exceed those of similar systems without SLS (16.5 and 6 %, respectively). This discrepancy emphasizes that SLS promotes the formation of active copper precipitation sites even at high copper (II) ion concentrations in solution.

Taken together, the data obtained confirm the pronounced positive effect of SLS on the interaction of pyrite with copper ions under hydrothermal conditions, manifested both in enhanced iron dissolution and in increased copper precipitation efficiency.

3.5. Characteristics of the Resulting Precipitates

Figure 7 shows X-ray diffraction patterns of the solid products obtained after the hydrothermal treatment of pyrite.

 doi:10.20944/preprints202512.1809.v1

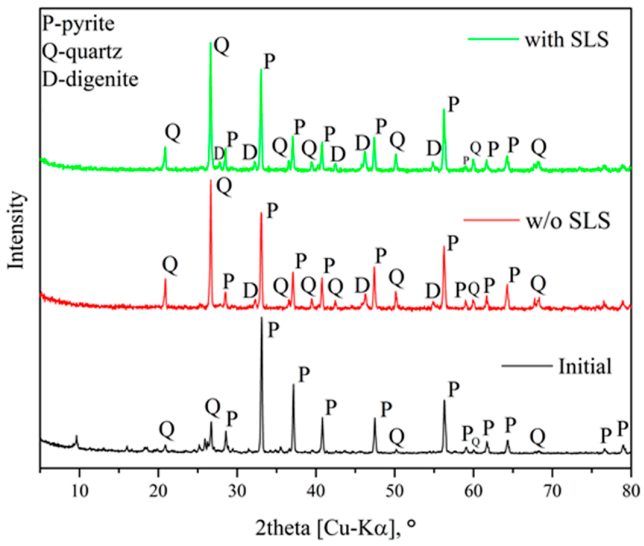

Figure 7. X-ray diffraction patterns of the solid products obtained after the hydrothermal treatment of pyrite.

According to the X-ray diffraction data, secondary copper sulfide digenite ($Cu_{1.8}S$) is formed during the hydrothermal reaction of pyrite, which is consistent with previously published results [32,35,50–53]. In the early stages of transformation or at low temperatures, the presence of CuS could be detected in the solid product, whereas at elevated temperatures or longer reaction times, the formation of $Cu_{1.8}S$ phase is observed.

Temperature has a significant effect on the degree of pyrite transformation and the reaction mechanism. No formation of Fe_2O_3, metallic copper, or other secondary phases is observed. The phase composition of the solid residue indicates that the pyrite transformation process proceeds predominantly according to Eqs (4–7). Similar to the results of [51], the presence of $Cu_{1.8}S$ is confirmed.

Based on these data, it can be concluded that pyrite transformation in copper sulfate solution occurs sequentially through the formation of the phases CuS → $Cu_{1.8}S$ → $Cu_{1.94}S$ → Cu_2S [35]. This sequence reflects the gradual enrichment of the sulfide layer with copper, which is consistent with the thermodynamically determined direction of the interaction processes between FeS_2 and Cu (II).

During hydrothermal treatment of pyrite in a $CuSO_4$ solution, the resulting layer of copper sulfides (CuS–$Cu_{1.8}S$) may shield the pyrite surface and reduce the rate of reaction due to a diffusion barrier associated with reagent access to the surface and impeding the removal of transformation products. The rate of diffusion through this product layer is determined primarily by its thickness, density, and porosity.

Scanning electron microscopy (SEM) was used to characterize the resulting precipitates. The results of analysis of the resulting precipitates from the hydrothermal treatment of pyrite with copper sulfate in the absence and presence of SLS at $[H_2SO_4]_0$ = 30 g/dm^3; t = 220 °C; $[SLS]_0$ = 1 g/dm^3, $[Cu]_0$ = 15 g/dm^3 are presented in Figure 8.

 doi:10.20944/preprints202512.1809.v1

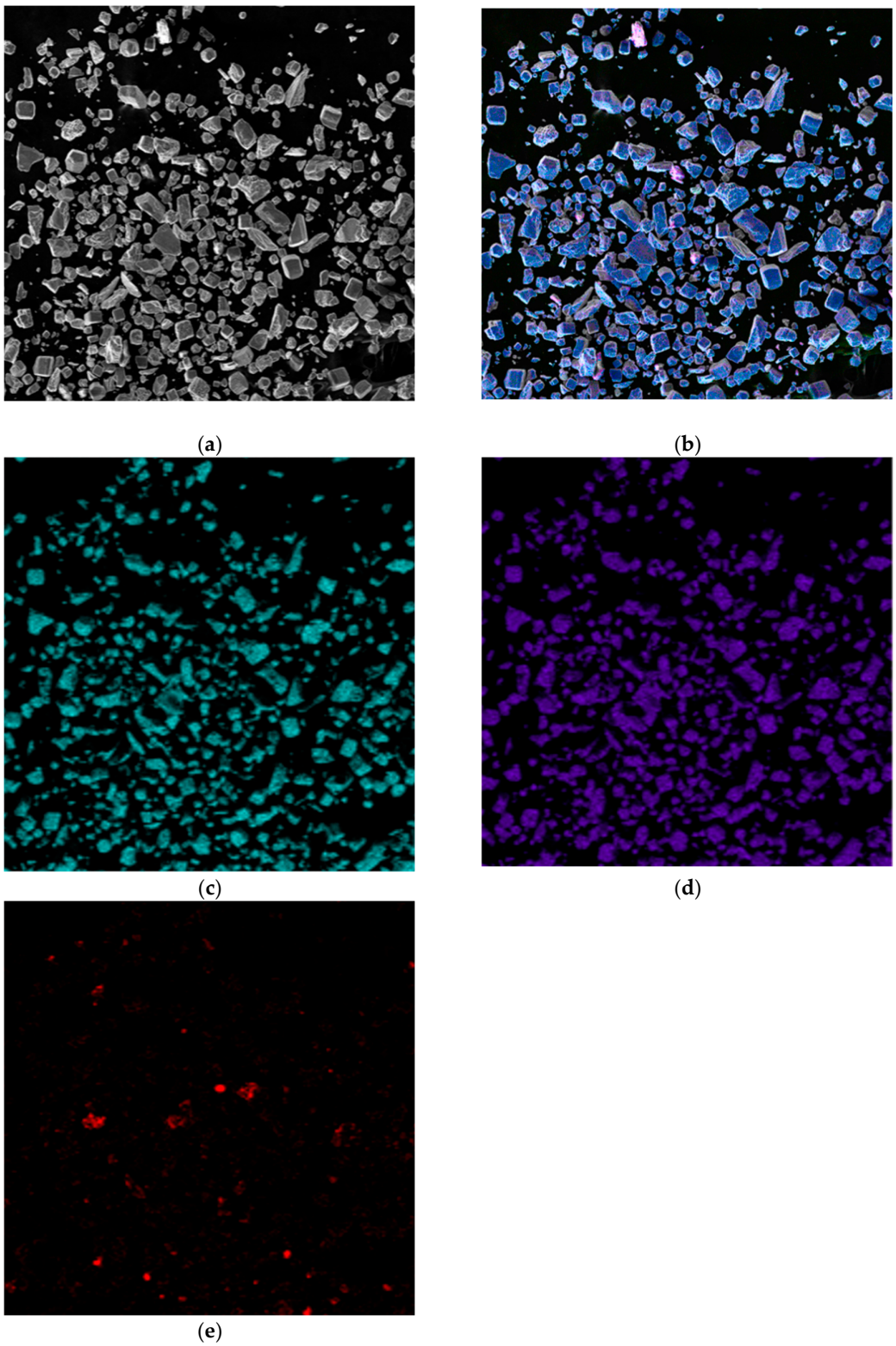

Figure 8. Micrograph and EDS mapping of pyrite cake without SLS (500 μm): (**a**) electron image, (**b**) – multilayer EDS image, (**c**) – EDS for sulfur, (**d**) – EDS for iron, (**e**) – EDS for copper).

Figure 8a shows cake particles for which the EDS map visualizes the distribution zones of the main elements: turquoise areas correspond to sulfur (Figure 8c), violet areas to iron (Figure 8d), and

 doi:10.20944/preprints202512.1809.v1

red areas to copper (Figure 8e). The overlap of turquoise and violet zones indicates the presence of pyrite, which is consistent with the morphology of the particles identified in Figure 8b.

The amount of copper deposited on pyrite is insignificant; its distribution is localized. Copper is observed primarily as individual small inclusions, irregularly dispersed across the surface of mineral particles. This is a typical feature of autoclave systems, where copper (II) ions are reduced to copper (I) and then precipitate as secondary sulfides on active surface areas.

When the image is zoomed in to 10 μm (Figure 9), it becomes apparent that the surface of most pyrite grains remains relatively smooth.

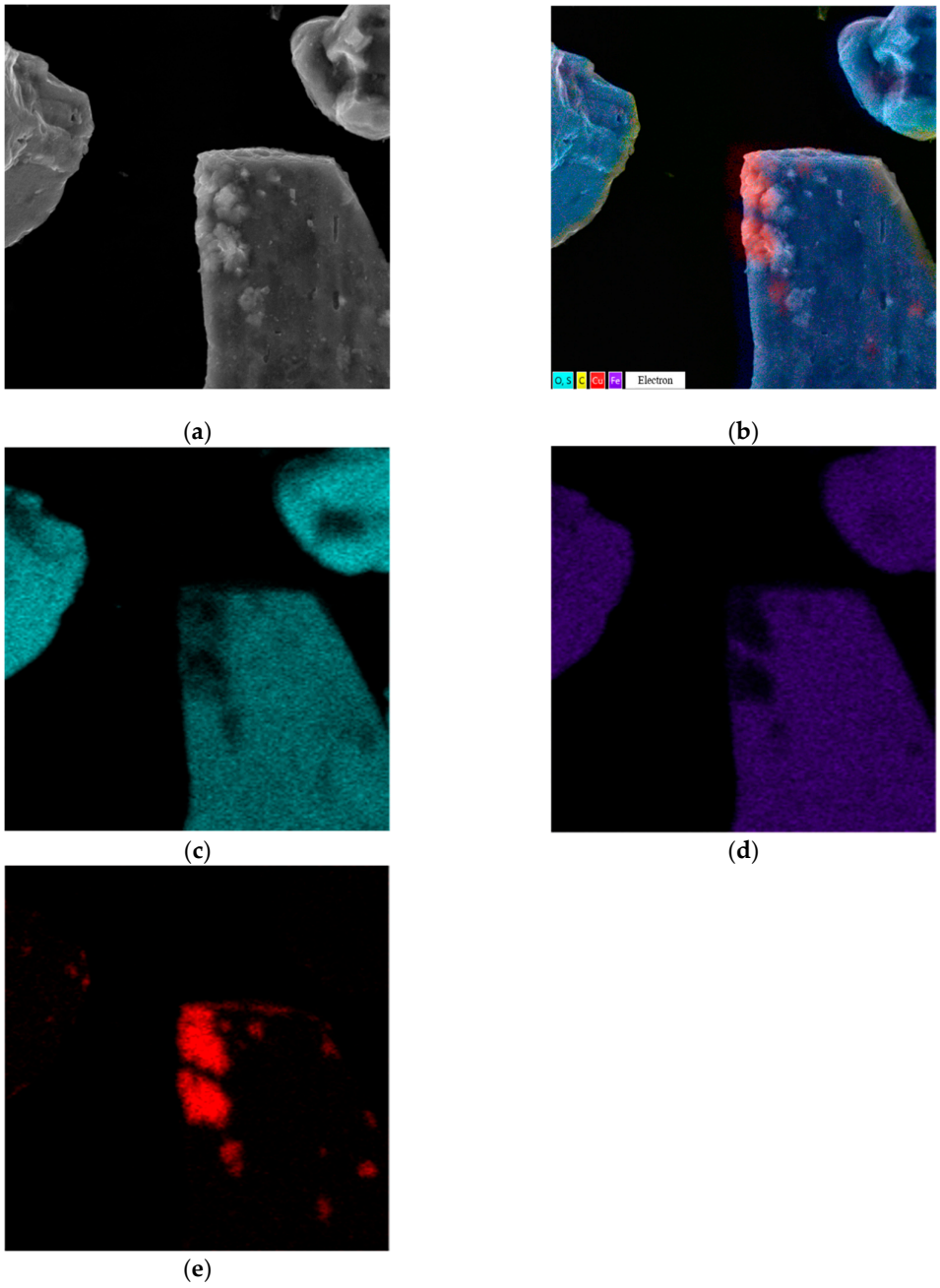

Figure 9. Micrograph and EDS mapping of the pyrite cake without SLS (10 μm): (**a**) electron image, (**b**) – multilayer EDS image, (**c**) – EDS for sulfur, (**d**) – EDS for iron, (**e**) – EDS for copper).

However, pronounced irregularities and microdepressions are observed in a number of localized areas. These morphological defects are due to the formation of secondary copper phase of

 doi:10.20944/preprints202512.1809.v1

digenite ($Cu_{1.8}S$). This is consistent with phase analysis data and general understanding of the mechanism of copper deposition on pyrite during hydrothermal oxidation.

This surface heterogeneity indicates that copper deposition is a point-like, nucleation process, controlled by localized electrochemical microzones and heterogeneities in the pyrite surface [54–60].

Analysis of the microstructure shown in Figure 9 suggests that secondary copper sulfides form predominantly in localized defect zones of the pyrite surface and are virtually nonexistent on smooth, low-activity areas of the particles. This spatial selectivity is characteristic of nucleation processes, where structural inhomogeneities, cracks, micropores, and areas with a disrupted crystal lattice act as nucleation centers.

The total copper particle content in the analyzed region does not exceed 4 %, confirming the limited nature of copper precipitation under these conditions. According to EDX mapping data (Figure 9b), the region where copper is localized (Figure 9e) is characterized by reduced sulfur content and a virtually complete absence of iron (Figure 9d). This combination is characteristic of secondary copper sulfides and possibly indicates the formation of compounds such as CuS, formed through the reduction of copper (II) ions and subsequent interaction with sulfur migrating within the surface layers of the mineral.

Thus, the morphology and distribution of elements in localized areas confirm that copper precipitates predominantly as secondary sulfides on pyrite surface defects, which act as active nucleation centers.

Micrographs and EDS mapping of a pyrite gas-extracted solid waste cake sample in the presence of SLS are shown in Figure 10.

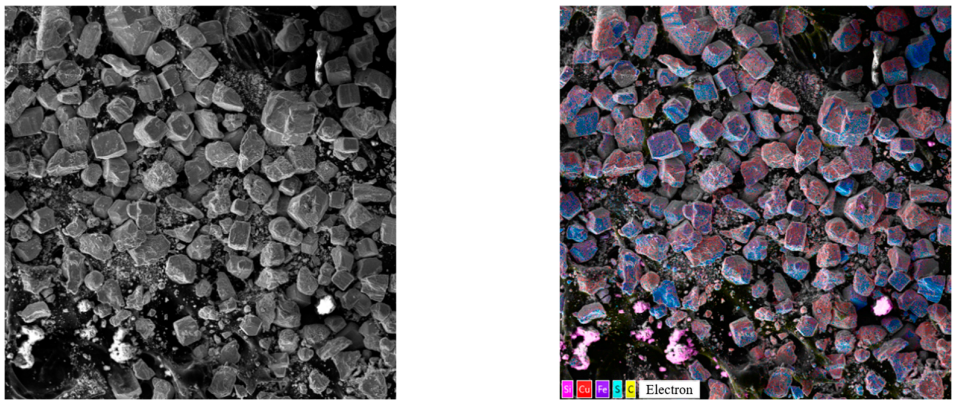

(**a**) (**b**)

(**c**) (**d**)

 doi:10.20944/preprints202512.1809.v1

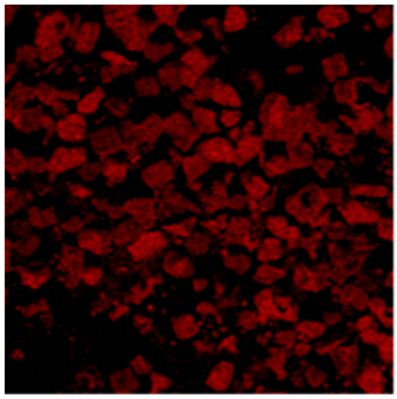

(**e**)

Figure 10. Micrograph and EDS mapping of a pyrite gas-extracted solid waste cake sample in the presence of SLS, 500 μm: (**a**) electron image, (**b**) – multilayer EDS image, (**c**) – EDS for sulfur, (**d**) – EDS for iron, (**e**) – EDS for copper).

According to the data presented in Figure 10, the addition of SLS leads to a significant change in the morphology of the solid products. The micrographs clearly show the appearance of a large number of small particles, which, as follows from the EDS mapping results, are most likely secondary copper sulfides. Their significant formation indicates that the presence of SLS promotes more intense interaction of copper (II) ions with pyrite on the surface, leading to its reduction and subsequent nucleation of secondary copper sulfides (CuS and $Cu_{1.8}S$) in the bulk of the suspension.

Furthermore, according to Figure 10e, the copper distribution on the pyrite surface becomes noticeably more uniform. Unlike the surfactant-free system, where copper precipitates as isolated point inclusions, individual inclusions are virtually nonexistent in the presence of SLS. This indicates a change in the precipitation mechanism. SLS likely prevents localized surface passivation by secondary copper sulfides and elemental sulfur, facilitating a more uniform transfer of copper ions to the pyrite surface, their interaction, and precipitation.

It can be noted that the iron signal intensity in the EDX maps significantly decreases, which may indicate partial shielding of the pyrite surface by secondary copper phases.

Micrographs of fine cake particles obtained in the presence of SLS are shown in Figure 11.

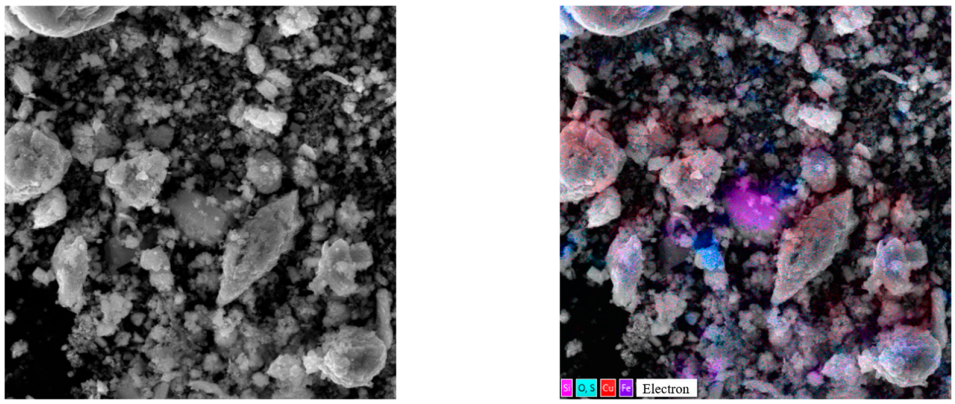

(**a**) (**b**)

 doi:10.20944/preprints202512.1809.v1

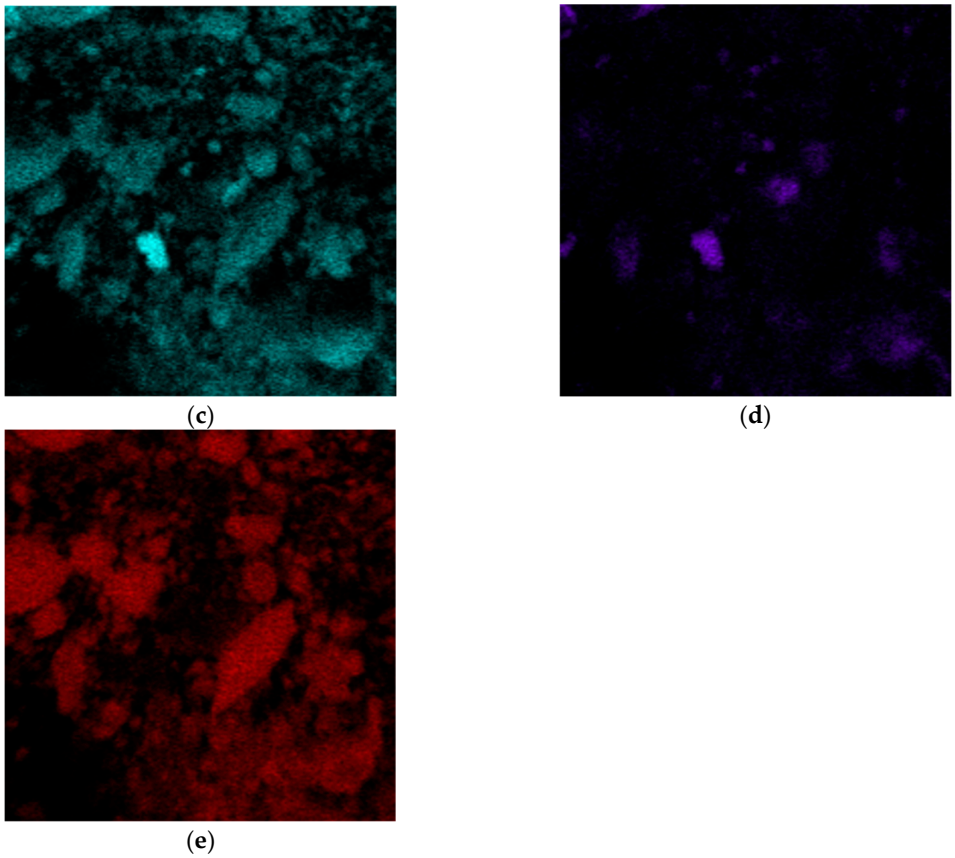

Figure 11. Micrographs and EDS mapping of a pyrite cake sample from a gas-extracted wastewater treatment plant in the presence of SLS, 10 μm: (**a**) electron image, (**b**) – multilayer EDS image, (**c**) – EDS for sulfur, (**d**) – EDS for iron, (**e**) – EDS for copper).

These particles have a significantly more developed and morphologically heterogeneous surface compared to the products formed in the system with no surfactants. This confirms the influence of SLS on the formation of secondary phases and the overall morphology of minerals during hydrothermal treatment.

As can be seen from the presented images (Figure 11), fine particles are formed primarily as a result of the interaction of copper ions with elemental sulfur, fine pyrite particles, and the subsequent separation of the formed copper sulfides. In the presence of SLS, the dispersion processes of sulfur and secondary phases are significantly enhanced, leading to the formation of a developed fine fraction. Almost all of the "fine" material is represented by secondary copper sulfides, which is clearly confirmed by the EDS maps (Figure 11d,e), which record the characteristic distribution of copper with a simultaneous almost complete absence of iron signals.

Nevertheless, fragments of unreacted pyrite are also found among the fine particles (Figure 11c, d). There are no signs of secondary copper phase precipitation on their surface. This suggests that previously formed copper sulfides may have separated from the pyrite surface during hydrothermal treatment. This effect is consistent with the observed morphology—smooth pyrite areas and the absence of copper inclusions indicate mechanical separation with the combined action of surfactants. The latter, due to its absorption and dispersive properties, concentrates on the pyrite surface, creating cracks and breaking large particles into small ones, while on the smaller particles, forming irregularities and roughness, facilitating the separation of newly formed copper sulfides from the surface.

Overall, the obtained microstructural data confirm that SLS significantly alters the mechanism of interaction between pyrite and copper and sulfur ions, promoting the formation of a finer phase

 doi:10.20944/preprints202512.1809.v1

of secondary copper sulfides and simultaneously influencing the distribution of copper among the mineral components of the solid product.

4. Conclusions

As can be seen from the presented images (Figure 11), fine particles are formed primarily as a result of the interaction of copper ions with elemental sulfur, fine pyrite particles, and the subsequent separation of the formed copper sulfides. In the presence of SLS, the dispersion processes of sulfur and secondary phases are significantly enhanced, leading to the formation of a developed fine fraction. Almost all of the "fine" material is represented by secondary copper sulfides, which is clearly confirmed by the EDS maps (Figure 11d,e), which record the characteristic distribution of copper with a simultaneous almost complete absence of iron signals.

The addition of SLS leads to a significant increase in the degree of iron extraction: at 200 °C for 120 min, the indicator increases from 14 % up to 26 %, and at 220 °C, up to 33.4 %. This confirms the increased dissolution of FeS_2 due to the prevention of passivation and improved access of Cu (II) to the mineral surface. The complex effect of SLS is expressed in the acceleration of redox exchange stages and increased mobility of the surface layers of the solid phase.

The most significant effect of SLS is manifested at the stage of Cu (I) reduction and precipitation: the degree of copper precipitation increases by 3–5 times. E.g., at 200 °C for 120 min, it increases from 5 % p to 23 %, and at 220 °C, from 6.7 % up to 26.8 %, respectively. SEM analysis shows that SLS promotes the formation of large arrays of secondary Cu sulfides and prevents the blocking of active pyrite sites.

Phase analysis has confirmed the sequential transformation $CuS \rightarrow Cu_{1.8}S$ – the classical pathway for the exchange substitution of pyrite by copper (II) ions. In the presence of SLS, the copper sulfide layer becomes less dense and more loose, which is consistent with the data from micrographs and SEM analysis.

Experimental data, X-ray phase analysis, and SEM/EDX showed that SLS radically changes the nature of the interaction of pyrite with copper (II) ions. The surfactant reduces the interfacial tension at the sulfur–solution boundary, preventing the formation of a continuous layer of elemental sulfur and secondary copper sulfides, improves the wetting of the FeS_2 surface and provides reagent access to the mineral's active sites. SEM morphology demonstrates a transition from localized point nucleation of copper sulfides to the uniform formation of a finely dispersed secondary phase across the surface and throughout the bulk of the suspension, confirming the elimination of diffusion barriers and mass transfer intensification.

In the absence of SLS, copper precipitation occurs locally, in defective zones of pyrite, forming individual $Cu_{1.8}S$/CuS inclusions. In the presence of SLS, a significantly more uniform copper distribution is observed, accompanied by the formation of finely dispersed secondary sulfide particles. SLS prevents localized surface passivation and promotes the initiation of Cu_xS formation over the entire particle surface, as well as the separation of secondary phases and their dispersion in the pulp. The solid phase morphology confirms the enhanced dynamics of sulfur and copper transfer in the system.

It has been demonstrated for the first time that SLS under hydrothermal conditions not only removes sulfur passivation but also actively regulates the mechanism of nucleation and growth of secondary copper sulfides, leading to the formation of a highly reactive dispersed phase and accelerated pyrite destruction. The established patterns are highly significant for the development of effective technologies for the chemical enrichment and recycling of pyrite-containing man-made materials, which can be effectively used for copper precipitation from industrial solutions with the production of commercial copper concentrates.

Author Contributions: Conceptualization, K.K and D.R.; methodology, K.K. and T.L.; software, M.T. and U.S.; validation, D.R., T.L. and K.K.; formal analysis, U.S. and M.T.; investigation, M.T.; resources, D.R.; data curation, K.K.; writing—original draft preparation, M.T. and O.D.; writing—review and editing, K.K., T.L. and D.R.;

 doi:10.20944/preprints202512.1809.v1

visualization, U.S., O.D. and M.T.; supervision, K.K.; project administration, K.K and D.R.; funding acquisition, K.K. and D.R. All authors have read and agreed to the published version of the manuscript.

Funding: This work was funded by the Russian Science Foundation under Project No. 25-79-10290 https://rscf.ru/project/25-79-10290. Analytical studies were carried out with the financial support of the State Task of the Russian Federation under Grant No. 075-03-2024-009/1 (FEUZ-2024-0010).

Data Availability Statement: The original contributions presented in the study are included in the article, further inquiries can be directed to the corresponding author.

Conflicts of Interest: The authors declare no conflicts of interest.

References

1. US Geological Survey. Copper Data Sheet—Mineral Commodity Summaries 2020; USGS: Reston, VA, USA, **2020**. Available online: https://pubs.usgs.gov/periodicals/mcs2020/mcs2020-copper.pdf (accessed on 15 October 2025).
2. Dreisinger, D. Copper leaching from primary sulfides: Options for biological and chemical extraction of copper. *Hydrometallurgy* **2006**, *83*, 10–20. https://doi.org/10.1016/j.hydromet.2006.03.032
3. International Copper Study Group. The World Copper Factbook 2019; ICSG: Lisbon, Portugal, **2020**. Available online: https://www.icsg.org (accessed on 15 October 2025).
4. Kelchevskaya, N.R.; Altushkin, I.A.; Korol, Yu.A.; Bondarenko, N.S. Peculiarities and importance of price formation in non-ferrous metallurgy (the case of copper concentrate production). *Tsvetnye Metally* **2016**, *8*, 13–19. https://doi.org/10.17580/tsm.2016.08.01.
5. Altushkin, I.A.; Vorob'ev, A.G.; Kelchevskaya, N.R.; Korol, Yu.A. Pricing in blister copper production: World market features and competitiveness requirements. *Tsvetnye Metally* **2017**, *12*, 7–11. https://doi.org/10.17580/tsm.2017.12.01.
6. Schlesinger, M.; Sole, K.; Davenport, W.; Alvear Flores, G. Extractive Metallurgy of Copper, 6th ed.; Elsevier: Amsterdam, The Netherlands, **2021**. https://doi.org/10.1016/C2019-0-03265-7
7. Gorai, B.; Jana, R.K.; Premchand. Characteristics and utilization of copper slag—A review. *Resour. Conserv. Recycl.* **2003**, *39*, 299–313. https://doi.org/10.1016/S0921-3449(02)00171-4.
8. Xu, B.; Ma, Y.; Gao, W.; Yang, J.; Yang, Y.; Li, Q.; Jiang, T. A review of the comprehensive recovery of valuable elements from copper smelting open-circuit dust and arsenic treatment. *JOM* **2020**, *72*, 3860–3875. https://doi.org/10.1007/s11837-020-04242-0.
9. Nazari, A.M.; Radzinski, R.; Ghahreman, A. Review of arsenic metallurgy: Treatment of arsenical minerals and the immobilization of arsenic. *Hydrometallurgy* **2016**, *174*, 258–281. https://doi.org/10.1016/j.hydromet.2016.10.011.
10. Lane, D.J.; Cook, N.J.; Grano, S.R.; Ehrig, K. Selective leaching of penalty elements from copper concentrates: A review. *Miner. Eng.* **2016**, *98*, 110–121. https://doi.org/10.1016/j.mineng.2016.08.006.
11. Wills, B.A.; Finch, J.A. Wills' Mineral Processing Technology: An Introduction to the Practical Aspects of Ore Treatment and Mineral Recovery, 8th ed.; Elsevier: Amsterdam, The Netherlands, **2016**. https://doi.org/10.1016/C2010-0-65478-2.
12. Voigt, S.; Szargan, R.; Suoninen, E. Interaction of copper(II) ions with pyrite and its influence on ethyl xanthate adsorption. *Surf. Interface Anal.* **1994**, *21*, 526–536. https://doi.org/10.1002/sia.740210804
13. Yılmaz, T.; Alp, İ.; Deveci, H.; Celep, O. Production of a copper concentrate by flotation from Yomra–Kayabasi massive Cu–Zn sulfide ore. *J. Sci. Technol. Dumlupinar Univ.* **2008**, *15*, 57–64. (In Turkish)
14. Chandra, A.P.; Gerson, A.R. A review of the fundamental studies of copper activation mechanisms for selective flotation of sphalerite and pyrite. *Adv. Colloid Interface Sci.* **2009**, *145*, 97–110. https://doi.org/10.1016/j.cis.2008.09.001.
15. Bıçak, Ö.; Ekmekçi, Z.; Can, M.; Öztürk, Y. The effect of water chemistry on froth stability and surface chemistry of flotation of a Cu–Zn sulfide ore. *Int. J. Miner. Process.* **2012**, *102–103*, 32–37. https://doi.org/10.1016/j.minpro.2011.09.005.
16. Xu, Z.; Zhang, Q.; Rao, S.R.; Finch, J.A. An in-plant test of sphalerite flotation without copper activation. In Proceedings of the 24th Annual CMP Conference; Ottawa, Canada, **1992**; Paper No. 14.

 doi:10.20944/preprints202512.1809.v1

17. Zhang, Q.; Xu, Z.; Bozkurt, V.; Finch, J.A. Pyrite flotation in the presence of metal ions and sphalerite. *Int. J. Miner. Process.* **1997**, *52*, 187–201. https://doi.org/10.1016/S0301-7516(97)00064-1
18. B.G. Lottermoser. Mine Wastes: Characterization, Treatment and Environmental Impacts, Third Ed., Springer, **2007**. https://doi.org/10.1007/978-3-642-12419-8
19. B.G. Lottermoser, Recycling, reuse and rehabilitation of mine wastes, Elements 7 (**2011**) 405–410, https://doi.org/10.2113/gselements.7.6.405.
20. Esposito, M.; Tse, T.; Soufani, K. Is the circular economy a new fast-expanding market? *Thunderbird Int. Bus. Rev.* **2017**, *59*, 9–14. https://doi.org/10.1002/tie.21764
21. Kossoff, D.; Dubbin, W.E.; Alfredsson, M.; Edwards, S.J.; Macklin, M.G.; Hudson-Edwards, K.A. Mine tailings dams: Characteristics, failure, environmental impacts, and remediation. *Appl. Geochem.* **2014**, *51*, 229–245. https://doi.org/10.1016/j.apgeochem.2014.09.010
22. Fernandes, G.W.; Goulart, F.F.; Ranieri, B.D.; Coelho, M.S.; Dales, K.; Boesche, N.; Soares-Filho, B. Deep into the mud: Ecological and socio-economic impacts of the Mariana dam breach (Brazil). *Natureza Conserv.* **2016**, *14*, 35–45. https://doi.org/10.1016/j.ncon.2016.10.003
23. Sequeira, C.A.C.; Santos, D.M.F.; Chen, Y.; Anastassakis, G. Chemical metathesis of chalcopyrite in acidic solutions. *Hydrometallurgy* **2008**, *92*, 135–140. https://doi.org/10.1016/J.HYDROMET.2008.02.012.
24. **Dizer, O.; Rogozhnikov, D.; Karimov, K.; Kuzas, E.; Suntsov, A.** Nitric Acid Dissolution of Tennantite, Chalcopyrite and Sphalerite in the Presence of Fe(III) Ions and FeS2. *Materials* **2022**, *15*, 1545. https://doi.org/10.3390/ma15041545
25. McDonald, R.G.; Li, J.; Austin, P. High-Temperature Pressure Oxidation of Low-Grade Nickel Sulfide Concentrate with Control of Residue Composition. *Minerals* **2020**, *10*, 249. DOI: 10.3390/min10030249
26. **Kuzas, E.; Rogozhnikov, D.; Dizer, O.; Karimov, K.; Shoppert, A.; Suntsov, A.; Zhidkov, I.** Kinetic Study on Arsenopyrite Dissolution in Nitric Acid Media by the Rotating Disk Method. *Miner. Eng.* **2022**, *187*, 107770. https://doi.org/10.1016/j.mineng.2022.107770
27. **Karimov, K.A.; Rogozhnikov, D.A.; Naboichenko, S.S.; et al.** Autoclave Ammonia Leaching of Silver from Low-Grade Copper Concentrates. *Metallurgist* **2018**, *62*, 783–789. https://doi.org/10.1007/s11015-018-0720-0
28. **Rogozhnikov, D.A.; Zakharian, S.V.; Dizer, O.A.; Karimov, K.A.** Nitric Acid Leaching of the Copper-Bearing Arsenic Sulphide Concentrate of Akzhal. *Tsvetnye Metally* **2020**, *8*, 11–17. https://doi.org/10.17580/tsm.2020.08.02
29. **Rogozhnikov, D.A.; Mamyachenkov, S.V.; Karelov, S.V.; Anisimova, O.S.** Nitric Acid Leaching of Polymetallic Middlings of Concentration. *Russ. J. Non-Ferr. Met.* **2013**, *54*, 440–442. https://doi.org/10.3103/S1067821213060242
30. Fuentes, G.; Viñals, J.; Herreros, O. Hydrothermal purification and enrichment of Chilean copper concentrates. Part 2: Behavior of bulk concentrates. *Hydrometallurgy* **2009**, *95*, 113–120. https://doi.org/10.1016/j.hydromet.2008.05.004.
31. Kritskii A.; Naboichenko S.; Karimov K.; Agarwal, V.; Lundström, M. Hydrothermal pretreatment of chalcopyrite concentrate with copper sulfate solution. *Hydrometallurgy* **2020**, *195*, 105359. https://doi.org/10.1016/j.hydromet.2020.105359.
32. Kritskii, A.; Fuentes, G.; Deveci, H. A Critical Review of Hydrothermal Treatment of Sulfide Minerals with Cu(II) Solution in H2SO4 Media. ***Hydrometallurgy*** **2025**, *231*, 106413.
33. Liu, Q.; Liao, Y.; Wu, M.; Jia, X. Acid-Free Ultrasonic-Enhanced Hydrothermal Leaching of Copper and Zinc from Polymetallic Sulfide Secondary Concentrates. ***Sep. Purif. Technol.*** **2025**, *378*, 134701. https://doi.org/10.1016/j.seppur.2025.134701
34. Peterson, R.D.; Wadsworth, M.E. Solid–solution reactions in the hydrothermal enrichment of chalcopyrite at elevated temperatures. In Proceedings of the EPD Congress; Warren, G.W., Ed.; TMS: Warrendale, PA, USA, **1994**; pp. 275–291.
35. Kritskii, A; Celep, O.; Yazici, E.; Deveci, H.; Naboichenko, S. Hydrothermal treatment of sphalerite and pyrite particles with $CuSO_4$ solution. *Minerals Engineering* **2022**, *180*, 107507. https://doi.org/10.1016/j.mineng.2022.107507

 doi:10.20944/preprints202512.1809.v1

36. Zhang, Y.; Li, W.; Cai, Y.; Qu, Y.; Pan, Y.; Zhang, W.; Zhao, K. Experimental investigation of the reactions between pyrite and aqueous Cu(I) chloride solution at 100–250 °C. *Geochimica et Cosmochimica Acta* **2021**, *298*, 1-20. https://doi.org/10.1016/j.gca.2021.01.018
37. dos Santos, E.C.; de Souza, C.B.; de Almeida, I.C.; Vieira, M.M.; Dutra, A.J.B. Pyrite Oxidation Mechanism by Oxygen in Aqueous Medium. *J. Phys. Chem.* C **2016**, *120*, 17527–17536. DOI: 10.1021/acs.jpcc.5b10949.
38. Rimstidt, J.D.; Vaughan, D.J. Pyrite Oxidation: A State-of-the-Art Assessment of the Reaction Mechanism. *Geochim. Cosmochim. Acta* **2003**, *67*, 873–880. DOI: 10.1016/S0016-7037(02)01165-1.
39. Jiang, H.; Zhang, H.; Liu, W.; Yang, T. Study on Dissolution and Passivation of Chalcopyrite under Pressurized Leaching in O2–H2O System by Electrochemical and Surface Analysis Methods. *Minerals* **2023**, *13*, 996. DOI: 10.3390/min13080996
40. Jiang, Q.; Yang, S.; Zheng, X.; Deng, J.; Zhu, X.; Liu, X.; Li, J. Lignosulphonates in Zinc Pressure Leaching: Improving Sulfur Dispersion and Stabilizing Residue Impurities. *J. Clean. Prod.* **2024**, *438*, 140355. DOI: 10.1016/j.jclepro.2023.140355
41. Tong, L.; Dreisinger, D. Interfacial Properties of Liquid Sulfur in the Pressure Leaching of Nickel Sulfide Concentrates above the Melting Point of Sulfur. *Miner. Eng.* **2009**, *22*, 456–461. DOI: 10.1016/j.mineng.2008.12.003
42. Tong, L.; Dreisinger, D. The Adsorption of Sulfur Dispersing Agents on Sulfur and Nickel Sulfide Concentrate Surfaces. *Miner. Eng.* **2009**, *22*, 445–450. DOI: 10.1016/j.mineng.2008.12.006.
43. Khazieva, Z.K.; Mamyachenko, S.V.; Aleksandrova, T.N. Surfactants Influence on Sphalerite Wetting during Zinc Concentrate Pressure Leaching. *Solid State Phenom.* **2017**, *265*, 1104–1108. DOI: 10.4028/www.scientific.net/SSP.265.1104
44. Aro, T.; Fatehi, P. Production and Application of Lignosulfonates and Sulfonated Lignin. *ChemSusChem* **2017**, *10*, 1861–1877. DOI: 10.1002/cssc.201700082.
45. Billich, A.; Kolo, H.; Uhlig, M.; Koch, C.; Niemeyer, J.; Pfeiffer, A. Deciphering Molar Mass Distributions of Lignosulfonates with Asymmetric Flow Field-Flow Fractionation. *ACS Sustain. Chem. Eng.* **2024**, *12*, 17385–17397. DOI: 10.1021/acssuschemeng.4c05074
46. Yang, S.; Jiang, Q.; Zheng, X.; Deng, J.; Zhu, X.; Liu, X.; Li, J. Behavior of Calcium Lignosulphonate under Oxygen Pressure Leaching of a Zinc Sulfide Concentrate. *Hydrometallurgy* **2024**, *230*, 106317. DOI: 10.1016/j.hydromet.2024.106317.
47. Wei, D.; Wang, Y.; Li, D.; Chen, M.; Luo, H. Effects of Temperature, Oxygen Partial Pressure and Calcium Lignosulphonate on Chalcopyrite Dissolution in Sulfuric Acid Solution. *Trans. Nonferrous Met. Soc. China* **2022**, *32*, 3368–3378. DOI: 10.1016/S1003-6326(22)65900-4
48. Ouyang, X.; Qiu, X.; Chen, P. Adsorption Characteristics of Lignosulfonates in Salt-Free and Electrolyte Solutions. *Biomacromolecules* **2011**, *12*, 1652–1659. DOI: 10.1021/bm200808p
49. Owusu, C.; Dreisinger, D.B. Interfacial Properties in Liquid Sulfur, Aqueous Zinc Sulfate and Zinc Sulfide Systems. *Hydrometallurgy* **1996**, *43*, 207–218. DOI: 10.1016/S0304-386X(96)90002-X
50. Zies, E.G.; Allen, E.T.; Merwin, H.E. Some reactions involved in secondary copper sulphide enrichment. *Econ. Geol.* **1916**, *11*, 407–503. https://doi.org/10.2113/gsecongeo.11.5.407.
51. Fuentes, G.; Viñals, J.; Herreros, O. Hydrothermal purification and enrichment of Chilean copper concentrates. Part 1: Behavior of bornite, covellite, and pyrite. *Hydrometallurgy* **2009**, *95*, 104–112. https://doi.org/10.1016/j.hydromet.2008.05.005.
52. Kritskii, A.; Naboichenko, S. Hydrothermal Treatment of Arsenopyrite Particles with CuSO4 Solution. ***Materials*** **2021**, *14*, 7472. https://doi.org/10.3390/ma14237472
53. Viñals, J.; Fuentes, G.; Hernandez, M.C.; Herreros, O. Transformation of sphalerite particles into copper sulfide particles by hydrothermal treatment with Cu(II) ions. *Hydrometallurgy* **2004**, *75*, 177–187. https://doi.org/10.1016/j.hydromet.2004.07.005
54. Chandra, A.P.; Puskar, L.; Simpson, D.J.; Gerson, A.R. Copper and xanthate adsorption onto pyrite surfaces: Implications for mineral separation through flotation. *Int. J. Miner. Process.* **2012**, *114–117*, 16–26. https://doi.org/10.1016/j.minpro.2012.08.003
55. Guo, B.; Peng, Y. The interaction between copper species and pyrite surfaces in copper cyanide solutions. *Int. J. Miner. Process.* **2017**, *158*, 85–92. https://doi.org/10.1016/j.minpro.2016.11.021

 doi:10.20944/preprints202512.1809.v1

56. Guo, B. Electrodeposition on pyrite from copper(I) cyanide electrolyte. *RSC Adv.* **2016**, *6*, 2183–2190. https://doi.org/10.1039/C5RA23948F
57. Weisener, C.; Gerson, A.R. An Investigation of the Cu(II) Adsorption Mechanism on Pyrite by ARXPS and SIMS. *Miner. Eng.* **2000**, *13*, 1329–1340. DOI: 10.1016/S0892-6875(00)00116-3.
58. von Oertzen, G.U.; Skinner, W.; Nesbitt, H.W.; Pratt, A.; Buckley, A.N. Cu Adsorption on Pyrite (100): Ab Initio and Spectroscopic Studies. *Surf. Sci.* **2007**, *601*, 5794–5799. DOI: 10.1016/j.susc.2007.06.060.
59. Yang, B.; Hu, Y.; Sun, W.; Sun, Y.; Gao, Z. Activation of Pyrite by Copper Ions and Its Depression by Thioglycollic Acid in the Flotation of a Complex Sulfide Ore. *Minerals* **2018**, *8*, 16. DOI: 10.3390/min8010016.
60. You, Y.; Hu, Y.; Sun, W.; Wang, D. Study of Galvanic Interactions between Pyrite and Chalcopyrite in a Flowing System. *Environ. Geol.* **2007**, *52*, 1093–1099. DOI: 10.1007/s00254-006-0444-5.